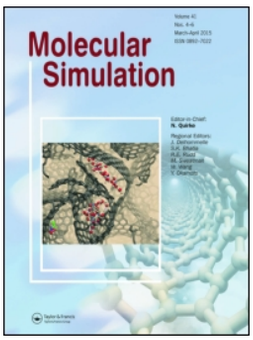

Molecular Simulation

ISSN: 0892-7022 (Print) 1029-0435 (Online) Journal homepage: http://www.tandfonline.com/loi/gmos20

Computation of elastic constants of solids using molecular simulation: comparison of constant volume and constant pressure ensemble methods

G. Clavier, N. Desbiens, E. Bourasseau, V. Lachet, N. Brusselle-Dupend & B. Rousseau

To cite this article: G. Clavier, N. Desbiens, E. Bourasseau, V. Lachet, N. Brusselle-Dupend & B. Rousseau (2017) Computation of elastic constants of solids using molecular simulation: comparison of constant volume and constant pressure ensemble methods, Molecular Simulation, 43:17, 1413-1422, DOI: 10.1080/08927022.2017.1313418

To link to this article: https://doi.org/10.1080/08927022.2017.1313418

MOLECULAR SIMULATION, 2017
VOL. 43, NO. 17, 1413–1422
https://doi.org/10.1080/08927022.2017.1313418

Taylor & Francis
Taylor & Francis Group

Computation of elastic constants of solids using molecular simulation: comparison of constant volume and constant pressure ensemble methods

G. Clavier[a,d], N. Desbiens[b], E. Bourasseau[b,c], V. Lachet[a,d], N. Brusselle-Dupend[a] and B. Rousseau[d]

[a]IFP Energies nouvelles, Rueil-Malmaison, France; [b]CEA, DAM, DIF, Arpajon, France; [c]CEA, DEN, DEC, Saint-Paul-lez-Durance, France; [d]Laboratoire de Chimie Physique, Université Paris-Sud, UMR 8000 CNRS, Orsay, France

ABSTRACT

We compute the elastic stiffness tensor of fcc argon at 60 K and 1 bar using molecular simulation tools. Three different methods are investigated: explicit deformations of the simulation box, strain fluctuations at constant pressure and stress fluctuations at constant volume. Statistical ensemble sampling is done using molecular dynamics and Monte Carlo simulations. We observe a good agreement between the different methods and sampling algorithms excepted with molecular dynamics simulations in the (NpT) ensemble. There, we notice a strong dependence of the computed elastic constants with the barostat parameter, whereas molecular dynamics simulations in the (NVT) ensemble are not affected by the thermostat parameter.

ARTICLE HISTORY
Received 27 January 2017
Accepted 24 March 2017

KEYWORDS
Molecular simulation; argon; elastic constants; stress fluctuation methods; strain fluctuation methods

1. Introduction

Mechanical properties tell us how materials behave under loading. Amongst them, elasticity describes how a material deforms under a given stress or how it will regain its original size and shape when the applied stress is removed. Today, many useful engineering materials are heterogeneous materials, composed of several different phases. Mechanical properties of these materials depend in a complex manner of the properties of the different phases, their morphology and the overall composition. This is the case, e.g. for polymer nanocomposites, polymer/clay composites or even electronic components [1–5].

In an effort to understand and predict the mechanical properties of such materials, micro-mechanical models have been developed [6]. The inputs for these models usually rely on pure phase properties, at a length scale where the phase may no longer behave isotropically. Although experiments can be done at such small length scales [7,8], molecular simulations directly give mechanical properties on the scale of a few nanometres. This has been a strong motivation for the development of predictive molecular simulation tools applied to mechanical properties and, over the years, several approaches have been derived to obtain the elastic stiffness tensor (also called elastic constant tensor) from molecular simulations. One method simply mimics experiments by evaluating the stress response [9,10] or the total potential energy [11] due to the application of a finite deformation to the simulated material. Using statistical mechanics, elastic stiffness tensor can also be related to spontaneous fluctuations of some observables in the system. Rahman and colleagues [12–14] were able to relate strain tensor fluctuations to the elastic stiffness tensor in different statistical ensembles. The shape of the simulation box must be allowed to change and some constant stress algorithm has to be used. Elastic stiffness tensor can also be related with stress tensor fluctuations [10,13,15] using constant volume simulations.

All the methods cited above can be used with molecular dynamics (MD) or Monte Carlo (MC) simulations, which are two different ways of sampling the configurational space of the system. In practice, the two methods are not fully equivalent. They differ at least by the way intensive parameters are fixed. In the MC procedure, intensive parameters are constant values used in the Metropolis criterion to weight explored configurations according to the thermodynamic potential of the concerned ensemble. As such, they are not explicitly calculated during the simulation. In MD, so-called *extended Hamiltonian* methods are used to maintain the system at a given pressure and/or temperature [16–21]. These algorithms are developed in order to reproduce as accurately as possible the phase space in the considered ensemble. However, these algorithms add new particles to the system, corresponding to the thermostat and the barostat. The mass of these particles must be carefully chosen as they affect spontaneous fluctuations in the system.

In this paper, we check how the statistical ensemble, as implemented in MC or MD, may influence the computed values of the elastic stiffness tensor. To this end, simulations were carried out on the fcc crystal of argon at 60 K and 1 bar. We also compare the efficiency of the different methods.

The paper is organised as follows: first, we present the different methods used in this work to compute the stiffness tensor. Second, we describe the argon model and the molecular simulation tools. As those methods are already well known, we emphasise here on practical details related to the computation of elastic properties. Finally, we present and discuss the results obtained from molecular simulations and compare them with previous simulations and available experimental data.

CONTACT B. Rousseau bernard.rousseau@u-psud.fr
Supplemental data for this article can be accessed here. [https://doi.org/10.1080/08927022.2017.1313418]

2. Computing the elastic stiffness tensor

In this section, we first define the elastic stiffness tensor **C**, then we introduce the operational equations that we used to compute it.

The elastic stiffness tensor is defined in the limit of small deformations. In this regime, there is a linear relationship between the deformation and the stress, as expressed by the generalised Hooke's law:

$$\sigma_{\alpha\beta} = C_{\alpha\beta\mu\nu}\,\epsilon_{\mu\nu} \tag{1}$$

where the implicit sum convention is used and where α, β, μ, ν represent the Cartesian coordinates, $\boldsymbol{\epsilon}$ is the strain tensor, $\boldsymbol{\sigma}$ is the stress tensor and **C** is the stiffness tensor, a fourth-rank tensor. The strain tensor elements give the change in an element of length when the body is deformed. For small deformations, strain tensor elements are equal to

$$\epsilon_{\alpha\beta} = \frac{1}{2}\left(\frac{\partial d_\alpha}{\partial r^0_\beta} + \frac{\partial d_\beta}{\partial r^0_\alpha}\right) \tag{2}$$

where $\mathbf{d} = \mathbf{r} - \mathbf{r}^0$ is the displacement of point **r** from its reference state $\mathbf{r}^0$.

From the thermodynamics of deformation, the stress tensor components $\sigma_{\alpha\beta}$ are obtained by derivating the free energy with respect to the components of the strain tensor, at constant temperature. In molecular simulations, the instantaneous stress tensor is usually computed using the virial theorem [22] as the opposite of the pressure tensor. The stress tensor is taken as the ensemble average of this quantity.

It can be easily shown that $\boldsymbol{\epsilon}$ and $\boldsymbol{\sigma}$ are symmetric tensors [23]. The Voigt notation is commonly used to represent symmetric tensors by reducing their order and simplify notations. Pairs of indices $\alpha\beta$ are written as singlets, with $xx = 1$, $yy = 2$, $zz = 3$, $yz = 4$, $xz = 5$ and $xy = 6$. Using this representation, $\boldsymbol{\epsilon}$ and $\boldsymbol{\sigma}$ can be written as vectors with six components and **C** as a 6 by 6 matrix. The generalised Hooke's law is then written:

$$\sigma_i = C_{ij}\epsilon_j \tag{3}$$

using implicit sum convention with $j = 1$ to 6 and $\epsilon_4 = 2\epsilon_{yz}$, $\epsilon_5 = 2\epsilon_{xz}$ and $\epsilon_6 = 2\epsilon_{xy}$ (see Appendix 1). Both complete and Voigt notations will be used throughout this paper.

2.1. Explicit deformation method

The explicit deformation method makes use of the generalised Hooke's law and is therefore valid only in the elastic regime (linear regime). It has been used for several decades in the molecular simulation community and is still in use today [3,24–28]. Basically, different types of deformations are applied to the simulation box. After equilibration, a long simulation is run to obtain the equilibrium stress tensor under a small deformation. The full set of C_{ij} elements can be extracted from several deformations.

In this work, we used six different deformation types, that we called *elementary deformations* because all elements of the strain tensor are zero but one. In this way, C_{ij} is directly the proportionality coefficient between the stress element σ_i and the strain element ϵ_j. For each type of deformation, we use different magnitudes of the deformation and extract C_{ij} from the slope of the corresponding stress–strain plot.

In the first deformation type, the box is elongated (or compressed) in the x direction by a relative quantity ξ. This deformation is accompanied by a volume change. During this elongation, each point in the periodic cell is transformed as follows:

$$\begin{pmatrix} x \\ y \\ z \end{pmatrix} \rightarrow \begin{pmatrix} x(1+\xi) \\ y \\ z \end{pmatrix} \tag{4}$$

The strain component ϵ_1 is trivially given by:

$$\epsilon_1 = \epsilon_{xx} = \frac{\partial}{\partial x}\left(x\xi\right) = \xi \tag{5}$$

and the strain tensor is $\boldsymbol{\epsilon} = (\epsilon_1, 0, 0, 0, 0, 0)$. Second and third deformation types are elongations identical to the first one, but for y and z directions, respectively.

The fourth deformation type is a shear strain. The orthorhombic box is deformed, at constant volume, into a monoclinic box by changing the angle α between **b** and **c** box vectors by a relative quantity ξ, i.e. α becomes $\alpha(1-\xi)$. During this shear, each point of the periodic cell is transformed as:

$$\begin{pmatrix} x \\ y \\ z \end{pmatrix} \rightarrow \begin{pmatrix} x \\ y + z\tan(\alpha\xi) \\ z \end{pmatrix} \tag{6}$$

The strain component ϵ_4 is trivially given by:

$$\epsilon_4 = 2\epsilon_{yz} = \frac{\partial}{\partial z}\left(z\tan(\alpha\xi)\right) = \tan(\alpha\xi) \tag{7}$$

and the strain tensor is $\boldsymbol{\epsilon} = (0, 0, 0, \epsilon_4, 0, 0)$. Fifth and sixth deformation types are identical to the first one, but applied to angles β and γ, respectively.

Finally, we recall below the expression used to compute the stress tensor [22] in MD simulations:

$$\sigma_{\alpha\beta} = -\frac{1}{V}\left[\sum_{i=1}^{N} m_i\, v_{\alpha,i} v_{\beta,i} + \sum_{i=1}^{N}\sum_{j>i}\left(-\frac{\partial u(r)}{\partial r}\right)_{r=r_{ij}} \frac{r_{\alpha,ij}\, r_{\beta,ij}}{\|\mathbf{r}_{ij}\|}\right] \tag{8}$$

where N is the total number of particles in the system, V the volume of the simulation box and $u(r)$ is the Lennard-Jones pair potential used in this study (see Equation (17)). m_i, $\mathbf{r}_i$ and $\mathbf{v}_i$ are, respectively, the mass, position and velocity of particle i. The vector $\mathbf{r}_{ij}$ is defined as $\mathbf{r}_i - \mathbf{r}_j$. In MC simulations, where particle velocities are not available, the kinetic term in Equation (8) is given by $Nk_BT\delta_{\alpha\beta}$ where T is the ensemble temperature, k_B is the Boltzmann constant and $\delta_{\alpha\beta}$ is the Kroenecker symbol.

2.2. Strain fluctuations at constant stress or constant pressure method

In 1981, Parrinello and Rahman proposed an MD algorithm to sample the isostress–isoenthalpic (NσH) ensemble [29]. In 1982, they demonstrated that strain fluctuations in the (NσH)

ensemble can be related to the adiabatic elastic stiffness tensor [12]. In 1985, Ray and Rahman [14] gave the following expression for the isothermal elastic stiffness tensor that can be used in isothermal–isostress (NσT) or isothermal–isobaric (NpT) ensemble:

$$C_{\alpha\beta\mu\nu} = \frac{k_B T}{\langle V \rangle} \left[\langle \epsilon_{\alpha\beta} \epsilon_{\mu\nu} \rangle - \langle \epsilon_{\alpha\beta} \rangle \langle \epsilon_{\mu\nu} \rangle \right]^{-1} . \quad (9)$$

In this equation, T is the temperature and $\langle V \rangle$ is the average simulation box volume. Equation (9) can be used in MC [30] or MD simulations. During MC simulations, box change moves, including box lengths and box angles (see Section 3.2 for details), are attempted. During MD, specific equations of motion have to be used to maintain temperature and stress tensor at a fixed value (see Section 3.3 for details).

To compute the strain tensor, we introduce the *scaling matrix*: $\mathbf{h} = \{\mathbf{a}, \mathbf{b}, \mathbf{c}\}$ where $\mathbf{a}$, $\mathbf{b}$ and $\mathbf{c}$ are the three vectors which span the molecular simulation cell. The $\mathbf{h}$ matrix describes the instantaneous size and shape of the simulation box. The box volume is related to $\mathbf{h}$ by the simple relation $V = \det(\mathbf{h})$. The strain tensor is given by

$$\boldsymbol{\epsilon} = \frac{1}{2} \left[\langle \mathbf{h} \rangle^{-1,\mathrm{T}} \, \mathbf{h}^{\mathrm{T}} \mathbf{h} \, \langle \mathbf{h} \rangle^{-1} - \mathbf{I} \right] \quad (10)$$

where $\langle \mathbf{h} \rangle$ is the ensemble average of $\mathbf{h}$ (or equivalently the reference box), $\mathbf{I}$ is the identity matrix, the superscript T means transposed matrix and the superscript -1 means inverse matrix. During the simulations, the norm of vectors $\mathbf{a}$, $\mathbf{b}$ and $\mathbf{c}$ are saved in a file along with the three angles α (between $\mathbf{b}$ and $\mathbf{c}$), β ($\mathbf{a}$ and $\mathbf{c}$) and γ ($\mathbf{a}$ and $\mathbf{b}$) to compute the strain tensor from Equation (10). The instantaneous scaling matrix is computed as follows:

$$\mathbf{h} = \begin{pmatrix} \|\mathbf{a}\| & \|\mathbf{b}\| \cos\gamma & \|\mathbf{c}\| \cos\beta \\ 0 & \|\mathbf{b}\| \sin\gamma & \frac{\mathbf{b}\cdot\mathbf{c} - b_x c_x}{b_y} \\ 0 & 0 & \left(\|\mathbf{c}\|^2 - c_x^2 - c_y^2 \right)^{1/2} \end{pmatrix} , \quad (11)$$

assuming $\mathbf{a}$ lies on the positive x axis, $\mathbf{b}$ is in the xy plane, with strictly positive y component and $\mathbf{c}$ may have any orientation with strictly positive z component.

2.3. Stress fluctuations at constant volume method

Squire et al. [31] have obtained an expression used to compute the isothermal elastic stiffness tensor in the canonical ensemble. Other derivations and details can be found in the work by Lutsko [15] or Van Workum et al. [32]. The elastic stiffness tensor is:

$$C_{\alpha\beta\mu\nu} = \langle C^{\mathrm{B}}_{\alpha\beta\mu\nu} \rangle - \frac{V}{k_B T} \left[\langle \sigma^{\mathrm{B}}_{\alpha\beta} \sigma^{\mathrm{B}}_{\mu\nu} \rangle - \langle \sigma^{\mathrm{B}}_{\alpha\beta} \rangle \langle \sigma^{\mathrm{B}}_{\mu\nu} \rangle \right] + \frac{N k_B T}{V} \left(\delta_{\alpha\mu}\delta_{\beta\nu} + \delta_{\alpha\nu}\delta_{\beta\mu} \right) \quad (12)$$

where $\sigma^{\mathrm{B}}_{\alpha\beta}$ is the Born contribution to the stress tensor

$$\sigma^{\mathrm{B}}_{\alpha\beta} = \frac{1}{V} \frac{\partial U}{\partial \epsilon_{\alpha\beta}} , \quad (13)$$

and $C^{\mathrm{B}}_{\alpha\beta\mu\nu}$ is the Born contribution to the elastic stiffness tensor

$$C^{\mathrm{B}}_{\alpha\beta\mu\nu} = \frac{1}{V} \frac{\partial^2 U}{\partial \epsilon_{\alpha\beta} \partial \epsilon_{\mu\nu}} . \quad (14)$$

The term U represents the potential energy in the system. Because of the stress fluctuation term in Equation (12), this method is often referred to as the stress-fluctuation method.

The first and second derivatives of the potential energy are computed during the simulation using the following expressions:

$$\frac{\partial U}{\partial \epsilon_{\alpha\beta}} = \sum_{i=1}^{N} \sum_{j>i} \left(\frac{\partial u(r)}{\partial r} \right)_{r=r_{ij}} \frac{r_{ij,\alpha} \, r_{ij,\beta}}{\|\mathbf{r}_{ij}\|} , \quad (15)$$

$$\frac{\partial^2 U}{\partial \epsilon_{\alpha\beta} \partial \epsilon_{\mu\nu}} = \sum_{i=1}^{N} \sum_{j>i} \left(\frac{\partial^2 u(r)}{\partial r^2} \right)_{r=r_{ij}} \frac{r_{ij,\alpha} \, r_{ij,\beta} \, r_{ij,\mu} \, r_{ij,\nu}}{\|\mathbf{r}_{ij}\|^2} - \left(\frac{\partial u(r)}{\partial r} \right)_{r=r_{ij}} \frac{r_{ij,\alpha} \, r_{ij,\beta} \, r_{ij,\mu} \, r_{ij,\nu}}{\|\mathbf{r}_{ij}\|^3} , \quad (16)$$

where $u(r)$ is the pair potential used in this study (see Equation (17) below). The Born contributions $\sigma^{\mathrm{B}}_{\alpha\beta}$ and $C^{\mathrm{B}}_{\alpha\beta\mu\nu}$ are saved during the course of the simulation and the elastic stiffness tensor is computed after run.

3. Model and molecular simulation tools

3.1. Molecular model for argon crystal

The system on which those methods were tested is a model of argon interacting through a Lennard-Jones 12-6 pair potential,

$$u(r) = 4\epsilon \left[\left(\frac{\sigma}{r} \right)^{12} - \left(\frac{\sigma}{r} \right)^{6} \right] , \quad (17)$$

with parameters $\epsilon/k_B = 119.8\,\mathrm{K}$ and $\sigma = 0.3405\,\mathrm{nm}$ [33]. A spherical cutoff $r_c = 1.2\,\mathrm{nm}$ is used for dispersion and repulsion interactions. The missing long range contributions to the energy and pressure are added, assuming a radial pair distribution function equal to unity above r_c [34]. Full periodicity is implemented in all space dimensions using the minimum image convention [34]. All simulations are realised in a cubic box containing $N = 500$ argon atoms initially located at the lattice sites of a face-centred cubic lattice. The initial lattice parameter value is 0.541 nm. This initial box is further relaxed at a temperature $T = 60\,\mathrm{K}$ and a pressure $P = 1\,\mathrm{bar}$, using MC simulations in the (NpT) ensemble (see details below). After equilibration, the lattice parameter value is $a = 0.53919\,\mathrm{nm}$. This value is in very good agreement with the X-ray data from Peterson et al. [35], $a = 0.53926\,\mathrm{nm}$, and also with X-ray data from Barrett and Meyer [36] where a least square fitting of the experimental diffraction data gives a value $a = 0.53925\,\mathrm{nm}$. This equilibrated box will be the starting configuration for all the mechanical studies.

3.2. MC simulations

The MC GIBBS code [37] was used in the canonical (NVT) and the isothermal–isobaric (NpT) ensembles. In the canonical ensemble, simple atomic translation moves are attempted and trial configurations are accepted with the following probability:

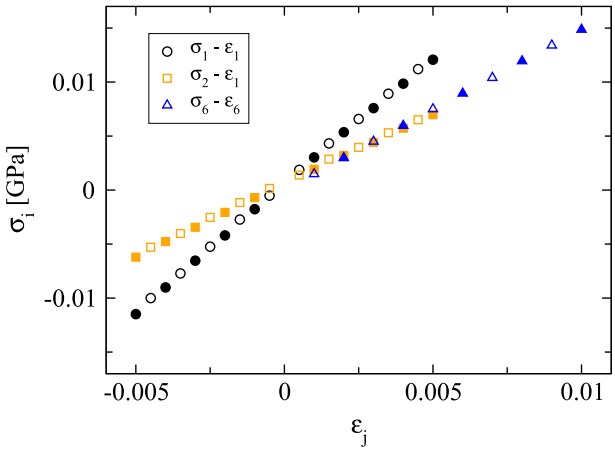

Figure 1. (Colour online) Stress–strain curves obtained from MC simulations (open symbols) and MD (full symbols). The Voigt notation is used for stress and strain elements. σ_1 and σ_2 were obtained using an uniaxial strain along the x direction, ϵ_1, and linear regression gives C_{11} and C_{21} terms, respectively. σ_6 was obtained using a shear strain associated with γ angle, ϵ_6, and linear regression gives the C_{66} term.

$$P_{\text{acc}} = \min\left\{1, \exp\left(-\Delta U/k_{\text{B}}T\right)\right\} \tag{18}$$

with $\Delta U = (U^{\text{new}} - U^{\text{old}})$ is the change in potential energy associated with the trial move and T is the ensemble temperature.

In the isothermal–isobaric ensemble, different moves are attempted and accepted with the probability [38]:

$$P_{\text{acc}} = \min\left\{1, \exp\left(\frac{-\Delta U - P\Delta V}{k_B T} + N \ln \frac{V^{\text{new}}}{V^{\text{old}}}\right)\right\} \tag{19}$$

with $\Delta V = (V^{\text{new}} - V^{\text{old}})$ is the change of volume associated with the trial move, P is the ensemble pressure and N is the number of atoms. Configurational sampling is realised using simple translation moves for individual atoms and global volume changes. In order to sample different box shapes, the following procedure was followed. A new attempted volume V^{new} is computed according to:

$$V^{\text{new}} = V^{\text{old}} + \Delta V^{\max}\left(2\zeta - 1\right) \tag{20}$$

where $\Delta V^{\max}$ is the maximum amplitude for volume change and ζ is a random number uniformly distributed between 0 and 1. Then, each volume change is randomly associated with a deformation of the box along a primary edge of the simulation box or, a change of angle between two primary edges and a deformation along the third primary edge. The new atom coordinates r_i^{new} are then computed using the following transformation:

$$\mathbf{r}_i^{\text{new}} = \mathbf{h}^{\text{new}}\,\mathbf{h}^{-1,\text{old}}\,\mathbf{r}_i^{\text{old}} \tag{21}$$

where $\mathbf{h}^{\text{new}}$ (respectively, $\mathbf{h}^{\text{old}}$) is the scaling matrix associated with the new (respectively, old) box shape, $\mathbf{h}^{-1}$ is the inverse of $\mathbf{h}$ and $\mathbf{r}_i^{\text{old}}$ is the old (before move) cartesian position vector of particle i. Typical attempt probabilities were 0.95 atomic translations and 0.05 volume changes.

3.3. Molecular dynamics

The LAMMPS code was used in the isothermal–isobaric ensemble. The LAMMPS code implements the Shinoda et al. [39] equations of motion to simulate volume change with box lengths and box angles fluctuations. The Shinoda equations of motion are equivalent to the Martyna et al. [21] implementation in the absence of external applied stress. The system is coupled with a Nosé–Hoover-type heat bath and a pressure bath, acting as thermostat and barostat, respectively. In this implementation, several variables are used to control the coupling between the baths and the particles. There are several thermostats (a chain) with mass Q_i^p, acting on particles, a barostat with mass W and optionally, another chain of thermostats with mass Q_i^b acting on the barostats. In LAMMPS code, all thermostat masses are related to a single input parameter which controls the relaxation time associated with these degrees of freedom, τ_T, whereas the barostat mass is controlled by the relaxation time τ_P. These two parameters act on kinetic energy and box shape fluctuations. We will see later how they affect the computation of the elastic stiffness tensor in the MD (NpT) ensemble.

The LAMMPS code was also used to apply small deformations (in the linear regime) to the simulation box. After deformation, the system was equilibrated in the canonical ensemble using the Nosé–Hoover chains thermostat.

Newton code [40] was used to compute the elastic stiffness tensor from stress fluctuations in the canonical ensemble. In this ensemble, Newton code implements the reversible Nosé–Hoover chains equations of motion as proposed by Martyna et al. [21]. The chain of thermostats is controlled by a single relaxation time τ_T.

In both LAMMPS and Newton codes, the equations of motion are integrated using the explicit reversible scheme from Martyna et al. [21]. Further details of the simulations will be given along with corresponding results.

4. Results

4.1. Explicit deformation simulations

In these numerical experiments, the reference orthorhombic box was first deformed using short MD runs of 10 ps. The following deformations were done:

- three elementary uniaxial strains (one for each spatial direction) with 5 positive ϵ_i values, in the range 0–0.5%, corresponding to a small extension of the material
- three elementary uniaxial strains (one for each spatial direction) with 5 negative ϵ_i values in the range −(0–0.5)%, corresponding to a small compression of the material
- three elementary shearing strains (one for each box angle) with 5 positive ϵ_i values in the range 0–1%.

Those 45 deformed boxes are then relaxed in the canonical ensemble in MD (100 ps) and MC (1 million steps). Finally, the average stress tensor for each box is computed in the canonical ensemble using a long production run of 10 ns in MD and 80 million steps in MC simulations. We present on Figure 1 typical stress–strain curves obtained from these MC and MD

simulations. As required, a linear regime is observed in the range of deformations investigated here.

Because of the cubic symmetry of the argon crystal, only three independent elastic constants are expected and **C** has the form of any isotropic material:

$$\mathbf{C} = \begin{pmatrix} C_{11} & C_{12} & C_{12} & 0 & 0 & 0 \\ C_{12} & C_{11} & C_{12} & 0 & 0 & 0 \\ C_{12} & C_{12} & C_{11} & 0 & 0 & 0 \\ 0 & 0 & 0 & C_{44} & 0 & 0 \\ 0 & 0 & 0 & 0 & C_{44} & 0 \\ 0 & 0 & 0 & 0 & 0 & C_{44} \end{pmatrix} \tag{22}$$

However, in an explicit deformation simulation, each C_{ij} element is obtained *independently* from the others and it is a good check to look at the full tensor. We present below the upper-left part of the C_{ij} tensor after uniaxial compressions using MD simulations. All values are expressed in GPa. Errors are confidence interval on the slope of σ_i vs. ϵ_j plot (see Appendix 2).

$$\begin{pmatrix} 2.43 \pm 0.04 & 1.38 \pm 0.03 & 1.34 \pm 0.02 \\ 1.37 \pm 0.02 & 2.42 \pm 0.04 & 1.37 \pm 0.05 \\ 1.38 \pm 0.05 & 1.36 \pm 0.03 & 2.46 \pm 0.03 \end{pmatrix}$$

Below is the lower-right part of the stiffness tensor obtained after shear deformations using MD simulations:

$$\begin{pmatrix} 1.49 \pm 0.01 & -0.01 \pm 0.00 & -0.01 \pm 0.01 \\ -0.00 \pm 0.01 & 1.50 \pm 0.01 & -0.00 \pm 0.02 \\ -0.01 \pm 0.01 & 0.00 \pm 0.02 & 1.49 \pm 0.01 \end{pmatrix}.$$

As can be seen, the shape of the matrix corresponds to the cubic symmetry, within statistical errors. The same behaviour was observed for all the simulations in this work. Therefore, in the following, we will call C_{11} the average $(C_{11} + C_{22} + C_{33})/3$, C_{44} the average $(C_{44} + C_{55} + C_{66})/3$ and C_{12} the average $(C_{12} + C_{13} + C_{21} + C_{23} + C_{31} + C_{32})/6$.

We present in Table 1 the average elastic constants obtained using the explicit deformation method. It is interesting to notice that significant differences are observed for elastic constants obtained from compression or extensional deformations. The argon crystal is stiffer when compressed rather than extended. This is a consequence of the shape of the Lennard-Jones 12-6 potential. This also demonstrates that although very small deformations are used (with magnitude close to spontaneous fluctuations), we cannot yet consider being in the limit of zero strain. However, a very good agreement is obtained between MD and MC values.

4.2. Constant pressure simulations

In these simulations, the reference orthorhombic box is run for 500 million steps using the MC GIBBS code in the (NpT) ensemble. Attempt probabilities are 95% translation moves and 5% volume change moves. Equivalent simulations are realised using the LAMMPS code in the (NpT) ensemble during 10 ns with a 1 fs timestep, a τ_T value of 0.1 ps and 10 elements for the Nosé–Hoover barostat and thermostat chains. τ_T value was chosen to reproduce as closely as possible kinetic energy fluctuations in the micro-canonical ensemble (observed from a further simulation, not described here). Seven different values were used for the time constant τ_P which controls the (NpT) barostat, ranging from 0.1 to 10.0 ps. MC and MD results obtained from the strain fluctuations expression (Equation (9)) are reported on Figure 2. Statistical errors were computed using the method of blocks (see Appendix 2 for details). MC results are represented as a

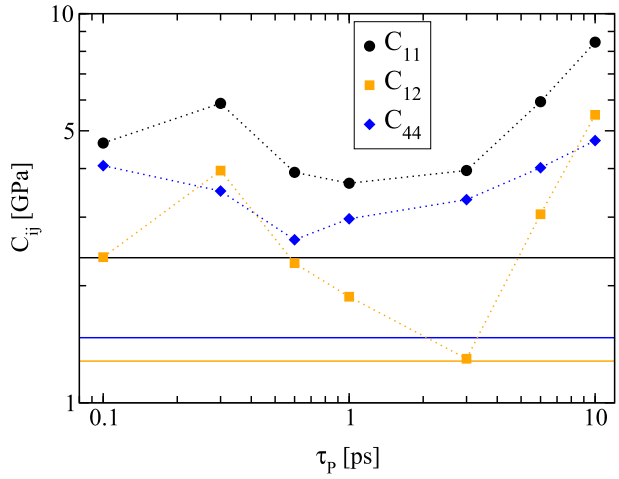

Figure 2. (Colour online) Elastic stiffness tensor elements C_{ij} computed from (NpT) simulations. MC simulations (straight lines) and MD simulations vs. τ_P (symbols). Statistical errors on C_{ij} values are smaller or equal to 0.02 GPa, which is of the order of the symbol size.

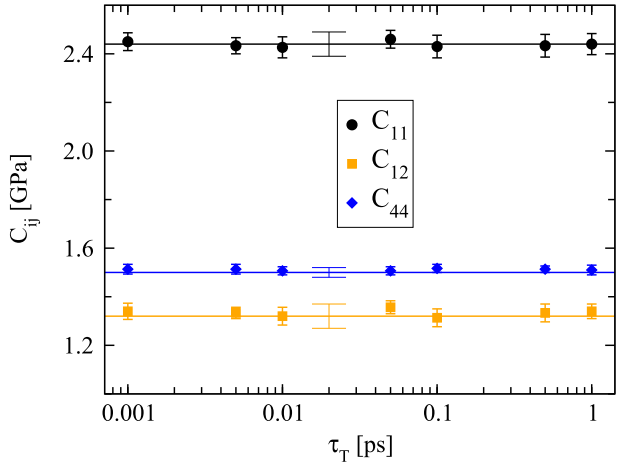

Figure 3. (Colour online) Elastic stiffness tensor elements C_{ij} computed from (NVT) simulations. MC simulations (straight lines) and MD simulations vs. τ_T (symbols). Statistical errors on C_{ij} MC values are indicated by thin lines at $\tau_T = 0.02$ ps.

Table 1. Average elastic constants, in GPa, obtained from MD and MC explicit deformation simulations. Keyword *comp* stands for uniaxial compression, *ext* stands for uniaxial extension, *ave* stands for average over compression and extension or for shear deformation.

		C_{11}	C_{12}	C_{44}
MD	comp	2.44 ± 0.04	1.37 ± 0.03	
	ext	2.28 ± 0.03	1.25 ± 0.03	
	ave	2.36 ± 0.04	1.31 ± 0.03	1.49 ± 0.01
MC	comp	2.41 ± 0.04	1.37 ± 0.04	
	ext	2.32 ± 0.04	1.28 ± 0.05	
	ave	2.36 ± 0.04	1.32 ± 0.04	1.49 ± 0.01

single line for each C_{ij} value. MC results are in very good agreement with the explicit deformation results presented above. On the contrary, MD results disagree with other simulation data. Computed C_{ij} values strongly depend upon the τ_P value. C_{12} changes by a factor of 4 in the studied range! More importantly, in the range of τ_P values studied here, the (NpT) MC values, and the MD/MC explicit deformation data, are not recovered. This means that the correct values for C_{ij} cannot be obtained with this method, at least when applied to Lennard-Jones solid systems. The reason for it can be understood from the change of box length and box angle fluctuations with τ_P. For example, box length standard deviation computed during the MD (NpT) run varies by more than 30% in the range of τ_P values used here. Consequently, **h** fluctuations and the strain covariance term appearing in Equation (9) depend on τ_P. The way C_{ij} depends on τ_P is not trivial and require further studies. Also, it will be interesting to test other MD barostats, as e.g. the Langevin barostat [41].

4.3. Constant volume simulations

In these simulations, the reference box is run for 800 million steps using the MC GIBBS code in the (NVT) ensemble with only translation moves. Equivalent simulations are realised using the Newton code in the (NVT) ensemble with Nosé–Hoover chains during 10 ns with a 1 fs timestep. Each chain is composed of 10 elements. We looked at the influence of different τ_T values, in the range 0.001–1 ps, on the predicted elastic constants. The comparison between MC and MD simulation results is given in Figure 3. Statistical errors were computed using the method of blocks (see Appendix 2 for details). An excellent agreement between MC and MD values is observed. Also, contrarily to what was observed in the (NpT) ensemble with τ_P values, we were not able to notice any influence of the Nosé–Hoover thermostat onto C_{ij} values.

5. Discussion

In this last section, we would like to discuss the efficiency and the convenience of use of the different methods presented here. We would like also to compare with previous results in the literature, concerning both simulations and experimental data.

As mentioned above, the explicit deformation method requires a tedious procedure in order to obtain the full elastic stiffness tensor, whereas with fluctuation methods, the tensor is obtained in a single simulation. In this work, we used a total number of 45 boxes to get the elastic tensor using explicit deformations. The whole procedure took a total computing time of 60 h with statistical errors of the order of 2%, whatever the sampling method, MD or MC. With the strain fluctuations at constant pressure method, 7 h are required using MC simulations to get the same statistical error. Using stress fluctuations at constant volume, MC simulations converged with a statistical error of the order of 5% in 7 h. Comparatively, using MD, the stress fluctuations at constant volume method gave of statistical error of 2% within 1 h. We conclude that the MD method at constant volume is the most efficient amongst the ones studied here, at least for the fcc crystal. If one considers the computation of mechanical properties of a system with a large number of particles, constant volume MD remains a good choice because parallelisation is more efficient than for MC codes. Obviously, the constant volume simulations require to include derivatives of the potential energy with respect to strain [32,42] into the molecular simulation code.

It should be mentioned that some improvement in convergence can be obtained using the fluctuation method as proposed by Gusev et al. [43] although the efficiency of the method is more pronounced at low temperature. Van Workum et al. [44] also proposed an enhanced MC sampling scheme, the *elastic bath method* with faster convergence of thermophysical properties over standard techniques. However, care must be taken when choosing the appropriate values of the elastic constants of the bath.

One of the main findings of this work is the difficulties encountered with MD simulations in the (NpT) ensemble, more precisely, the sensitivity of the elastic constants to the mass of the barostat. It is a surprising result, because this point is not mentioned in the literature. Nevertheless, we were not able to find a publication with a systematic study of the effect of τ_P on C_{ij}. In 1984, Sprik et al. [9] computed adiabatic elastic constants of the nearest neighbour Lennard-Jones model. They used MD in the NpH ensemble (isobaric–isoenthalpic ensemble from Parrinello and Rahman [29]). They mentioned that the mass of the barostat was taken identical to the mass of argon atom, 'which yields an optimal coupling between the motion of the boundaries of the MD cell and the particles of the system'. These data were compared with Cowley [45] values. Cowley did MC simulations in the (NVT) ensemble. He computed isothermal elastic constants and obtained adiabatic values using thermodynamic relationships. Although there is an important dispersion of C_{ij} values obtained by Sprik et al. (they worked with several boxes), the overall agreement with Cowley values is good. Furthermore, Sprik et al. also computed C_{ij} using stress–strain relations which confirmed the (NpH) data. In 1992, Fay and Ray [30] used strain fluctuations in the (NpH) ensemble to study the nearest neighbour Lennard-Jones model. They compared MC and MD simulations and found adiabatic elastic constants in very good agreement. They do not mention the mass used for the barostat. In the same paper [30], they report older data [10,46,47] obtained using MD in the (NVT) and (NVE) ensembles, also in good agreement with the (NpH) values and the ones from Cowley [45]. Our findings using a standard Lennard-Jones model are thus not consistent with these older works.

Finally, we would like to compare our values with literature values, both from simulation and experiments. So far, most of the molecular simulation studies were conducted on the nearest neighbour Lennard-Jones model [9,10,30,43–47]. This model has a very short cutoff radius which changes its thermodynamic behaviour compared with a standard Lennard-Jones model with typical cutoff radius 2.5 times the Lennard-Jones parameter σ or larger. In particular, the melting temperature of the model is close to a reduced temperature $0.5\epsilon/k_B$ and the model is much softer than argon at the same temperature. Interestingly, Squire et al. [31], as early as 1969, considered a cutoff larger than 2.5σ and computed explicitly isothermal elastic constants for a 108 atom argon fcc crystal. More recently, Quesnel et al. [25] used explicit deformations (constrained tension tests) on a 256

Table 2. Average isothermal elastic constants obtained using molecular simulations. Explicit deformation simulations took 450 ns with MD, 3.6×10^9 MC moves. (NpT) ensemble simulations took 10 ns with MD and 0.8×10^9 MC steps. (NVT) ensemble simulations took 10 ns with MD and 0.5×10^9 MC steps.

	C_{11}	C_{12}	C_{44}
Squire, 1969	2.28 ± 0.10	1.31 ± 0.06	1.44 ± 0.07
Quesnel, 1993	2.84	1.43	1.73
Explicit deformation			
MD	2.36 ± 0.04	1.31 ± 0.03	1.49 ± 0.01
MC	2.36 ± 0.04	1.32 ± 0.04	1.49 ± 0.01
Strain fluctuations in (NpT) ensemble			
MD $\tau_P = 1$ ps, $\tau_T = 0.1$ ps	3.66 ± 0.02	1.87 ± 0.02	3.47 ± 0.02
MC	2.36 ± 0.01	1.28 ± 0.01	1.47 ± 0.01
Stress fluctuations in (NVT) ensemble			
MD, $\tau_T = 0.1$ ps	2.43 ± 0.02	1.31 ± 0.04	1.52 ± 0.02
MC	2.44 ± 0.05	1.32 ± 0.05	1.50 ± 0.01

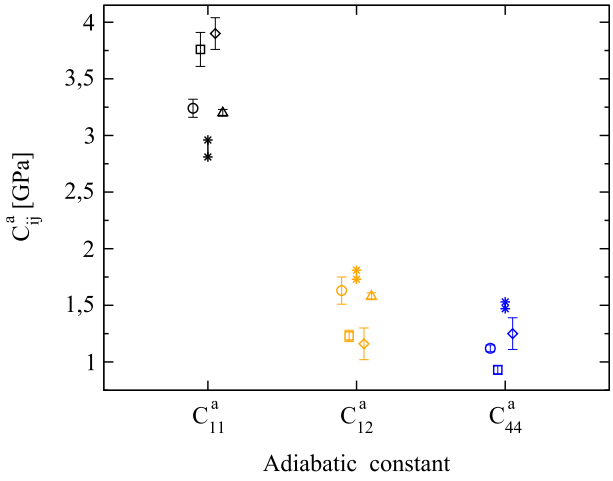

Figure 4. (Colour online) Adiabatic elastic constant tensor elements C^a_{ij}. Experimental values from Moeller (squares), Gsänger (diamonds), Keeler (circles) and Meixner (triangles up). Stars encompass the smaller and larger simulated values (strain fluctuation MD values are excluded).

atom fcc crystal. Their results along with our simulation data are reproduced in Table 2, including statistical uncertainties. Note that *relative* statistical errors are greater for C_{12} compared to C_{11} and C_{44} values, indicating a slower convergence for this off-diagonal element. If one excepts the strain fluctuations MD results, we observe a very good agreement with Squire et al. [31]. The values by Quesnel et al. [25] seem to overestimate the elastic constants of the model. They have been obtained using a constant-rate relative deformation of 2×10^{-6} per MD time step which may be considered as an upper value as a deformation of 0.5% is attained in 2500 time steps.

There have been several experimental studies on argon single crystal to measure elastic constants in a large temperature range. These studies are mostly based on sound velocity measurements. Moeller and Squire [48] used pulse echo technique to measure the sound velocity 'on an essentially single crystal' from 74 to 83.8 K. They used the data of Jones and Sparkes [49] to extrapolate velocity values from 18 to 62 K. Gsänger et al. [50] performed longitudinal sound velocity measurements on two argon single crystals in the range of 4.2–76.8 K. Keeler and Batchelder [51] were able to grow single crystals of argon of 1 cm diameter. They used the pulse echo technique to measure longitudinal and transverse waves from 3 to 77 K. Meixner et al. [52] studied the temperature dependence of the longitudinal sound velocity in a single crystal of argon by stimulated Brillouin scattering, from 4.2 to 77 K. Using the sound velocity, adiabatic elastic constants are measured. In order to compare our values with laboratory one, we computed adiabatic C^a_{ij} terms from isothermal values of Table 2 using the expressions given by Hoover et al. [53]:

$$C^a_{11} = C_{11} + \gamma^2 T \rho C_v \tag{23a}$$

$$C^a_{12} = C_{12} + \gamma^2 T \rho C_v \tag{23b}$$

$$C^a_{44} = C_{44} \tag{23c}$$

where γ is the Grüneisen gamma, ρ is the number density and C_v is the molar specific heat at constant volume. The quantity $\gamma^2 T \rho C_v$ is found to be 0.45 GPa at 60 K and zero pressure in Hoover's work [53], based on MC simulations. We also computed it from experimental values at 60 K and zero pressure given in Dobbs et al. [54] and found a very close value of 0.43 GPa. Figure 4 is a comparison between the experimental adiabatic elastic constant and those deduced from this work. As can be seen on Figure 4, there is a certain amount of disparity in the experimental values, though it appears that computed C_{11} is underestimated by roughly 25% whereas C_{12} and C_{44} look slightly overestimated. Although the Lennard-Jones model predicts well thermodynamic properties of argon, some discrepancies are seen for mechanical ones.

This disagreement is partially hindered when one computes the isothermal compressibility χ_T of a polycrystalline sample, because of error compensations. Indeed, the isothermal compressibility is computed from (isothermal) C_{11} and C_{12} using the following expression:

$$\chi_T = \frac{3}{C_{11} + 2C_{12}} \,. \tag{24}$$

Dobbs et al. [54] measured an isothermal compressibility of solid argon at 60 K of 0.585 GPa^{-1} and Peterson et al. [35] obtained an experimental value of 0.59 GPa^{-1} whereas explicit deformation MD simulations give a value of 0.61 ± 0.01 GPa^{-1} and explicit deformation MC simulations a value of 0.59 ± 0.01 GPa^{-1}.

The same conclusion applies for the shear modulus G. The macroscopic shear modulus of a polycrystalline sample can be computed from the elastic stiffness tensor $\mathbf{C}$ of a single crystal using a spatial averaging over possible lattice orientations. The two methods of averaging due to Voigt and Reuss lead to lower and upper limits for the experimental values of G. Hill [55] found that $G_H = (G_V + G_R)/2$ is very close to the experimental value for many materials, where $G_V = \left[(C_{11} - C_{12}) + 3C_{44}\right]/5$ and $G_R = 5\left[4/(C_{11} - C_{12}) + 3/C_{44}\right]$. We computed the shear modulus G based on C_{11}, C_{12} and C_{44} values using Hill approximation. Depending on the simulation method used, values are in the range 0.98 ± 0.02–1.03 ± 0.03 GPa. Dobbs reports a value of $G = 0.95$ GPa from ultrasonic velocity measurements in polycrystalline material. Our results for the shear modulus G are

thus within roughly 5% of the experimental data, a reasonably good agreement.

6. Conclusion

We have computed the elastic stiffness tensor of argon single crystal at 60 K and 1 bar using different molecular simulation approaches. Our results are in good agreement with Squire et al. computations [31]. Much more results are available in the litterature for the nearest neighbour Lennard-Jones model, but they cannot be used here for quantitative comparison purpose. Comparison of our data with experimental values deduced from sound velocity experiments reveals that the Lennard-Jones model underestimates C_{11} element by roughly 25% and slightly overestimates C_{12} and C_{14}. A better agreement with experiments is observed with isothermal compressibility χ_T or shear modulus G obtained from C_{ij} elements because of error compensations. This suggests that force field improvements have to be done by considering elastic tensor elements rather than bulk properties.

However, the most important finding of this study is related with the MD simulations in the (NpT) ensemble. Although all other simulation methods are in very good agreement, the strain fluctuation method gives poor results when MD is used on Lennard-Jones solid systems: when using the Nosé–Hoover based barostat in LAMMPS, C_{ij} values depend on the barostat parameter τ_P and the correct value (i.e. the value obtained by all other methods) cannot be recovered, whatever the τ_P value used. This is really a surprising result. As mentioned above, it contradicts in some part the conclusions reported by Fay and Ray [30] where MC and MD simulations, at constant volume or at constant pressure, are in good agreement. The main difference is the use of the isobaric–isoenthalpic ensemble from Parrinello and Rahman rather than the (NpT) ensemble used here. In a recent paper, Shirts [56] investigated the quality of standard pressure control algorithms for MD. From a study on water model, he concludes that 'typical aqueous simulations using Martyna–Tuckerman–Tobias–Klein may be more consistent with an (NpT) ensemble than Parrinello–Rahman... However, this test is with homogeneous fluids; it is possible that with an inhomogeneous system, other artefacts might appear'. Rogge et al. [57] investigated several barostats for the mechanical characterisation of metal–organic frameworks. They mention that dynamical properties that are directly related to cell fluctuations cannot be well reproduced by any barostat tried. We conclude that uncertainties still remain concerning the ability of (NpT) simulations using the Martyna et al. [21] or other algorithm to produce consistent data for elastic stiffness. Nevertheless, elastic constants can safely be determined using explicit deformation or constant volume simulations, using MD or MC simulations.

Disclosure statement

No potential conflict of interest was reported by the authors.

Supplementary material

LAMMPS (December 9, 2014 version) input files for NPT simulations are provided as supplementary material. The command file in.system and the data file data.system are given.

References

[1] Pinnavaia TJ, Beall GW. Polymer-clay nanocomposites. London: Wiley; 2001.

[2] den Toonder JMJ, van Dommelen JAW, Baaijens FPT. The relation between single crystal elasticity and the effective elastic behaviour of polycrystalline materials: theory, measurement and computation. Model Simul Mater Sci Eng. 1999 Nov;7(6):909–928.

[3] Griebel M, Hamaekers J. Molecular dynamics simulations of the elastic moduli of polymer–carbon nanotube composites. Comput Methods Appl Mech Eng. 2004 May;193(17–20):1773–1788.

[4] Sheng N, Boyce MC, Parks DM, et al. Multiscale micromechanical modeling of polymer/clay nanocomposites and the effective clay particle. Polymer. 2004 Jan;45(2):487–506.

[5] Zeng QH, Yu AB, Lu GQ. Multiscale modeling and simulation of polymer nanocomposites. Prog Polym Sci. 2008 Feb;33(2):191–269.

[6] Tucker III CL, Liang E. Stiffness predictions for unidirectional short-fiber composites: review and evaluation. Compos Sci Technol. 1999 Apr;59(5):655–671.

[7] Treacy MMJ, Ebbesen TW, Gibson JM. Exceptionally high Young's modulus observed for individual carbon nanotubes. Nature. 1996 Jun;381(6584):678–680.

[8] Lee C, Wei X, Kysar JW, et al. Measurement of the elastic properties and intrinsic strength of monolayer graphene. Science. 2008 Jul;321(5887):385–388.

[9] Sprik M, Impey RW, Klein ML. Second-order elastic constants for the Lennard–Jones solid. Phys Rev B. 1984 Apr;29(8):4368–4374.

[10] Ray JR. Elastic constants and statistical ensembles in molecular dynamics. Comput Phys Rep. 1988 Aug;8(3):109–151.

[11] Theodorou DN, Suter UW. Atomistic modeling of mechanical properties of polymeric glasses. Macromolecules. 1986 Jan;19(1):139–154.

[12] Parrinello M, Rahman A. Strain fluctuations and elastic constants. J Chem Phys. 1982;76(5):2662–2666.

[13] Ray JR, Rahman A. Statistical ensembles and molecular dynamics studies of anisotropic solids. J Chem Phys. 1984;80(9):4423–4428.

[14] Ray JR, Rahman A. Statistical ensembles and molecular dynamics studies of anisotropic solids. II. J Chem Phys. 1985 May;82(9):4243–4247.

[15] Lutsko JF. Generalized expressions for the calculation of elastic constants by computer simulation. J Appl Phys. 1989;65(8):2991–2997.

[16] Andersen HC. Molecular dynamics simulations at constant pressure and/or temperature. J Chem Phys. 1980;72(4):2384–2393.

[17] Nosé S. A unified formulation of the constant temperature molecular dynamics methods. J Chem Phys. 1984;81(1):511–519.

[18] Hoover WG. Canonical dynamics: equilibrium phase-space distributions. Phys Rev A. 1985 Mar;31(3):1695–1697.

[19] Martyna GJ, Klein ML, Tuckerman M. Nosé–Hoover chains: the canonical ensemble via continuous dynamics. J Chem Phys. 1992;97(4):2635–2643.

[20] Martyna GJ, Tobias DJ, Klein ML. Constant pressure molecular dynamics algorithms. J Chem Phys. 1994;101(5):4177–4189.

[21] Martyna GJ, Tuckerman ME, Tobias DJ, et al. Explicit reversible integrators for extended systems dynamics. Mol Phys. 1996 Apr;87(5):1117–1157.

[22] Irving JH, Kirkwood JG. The statistical mechanical theory of transport processes. IV. The equations of hydrodynamics. J Chem Phys. 1950;18(6):817–829.

[23] Landau LD, Lifshitz EM. Theory of elasticity, Course of theoretical physics, Vol. 7. London: Pergamon Press; 1959.

[24] Holt AC, Hoover WG, Gray SG, et al. Comparison of the lattice-dynamics and cell-model approximations with Monte-Carlo thermodynamic properties. Physica. 1970 Oct;49(1):61–76.

[25] Quesnel DJ, Rimai DS, DeMejo LP. Elastic compliances and stiffnesses of the fcc Lennard–Jones solid. Phys Rev B. 1993 Sep;48(10):6795–6807.

[26] Manevitch OL, Rutledge GC. Elastic properties of a single lamella of montmorillonite by molecular dynamics simulation. J Phys Chem B. 2004 Jan;108(4):1428–1435.

[27] Vashishta P, Kalia RK, Nakano A, et al. Interaction potential for silicon carbide: a molecular dynamics study of elastic constants and vibrational density of states for crystalline and amorphous silicon carbide. J Appl Phys. 2007;101(10):103515-1–103515-12.
[28] Pei Q-X, Zhang Y-W, Shenoy VB. Mechanical properties of methyl functionalized graphene: a molecular dynamics study. Nanotechnology. 2010 Feb;21(11):115709-1–115709-8.
[29] Parrinello M, Rahman A. Polymorphic transitions in single crystals: a new molecular dynamics method. J Appl Phys. 1981;52(12):7182–7190.
[30] Fay PJ, Ray JR. Monte Carlo simulations in the isoenthalpic-isotension-isobaric ensemble. Phys Rev A. 1992 Oct;46(8):4645–4649.
[31] Squire DR, Holt AC, Hoover WG. Isothermal elastic constants for argon. Theory and Monte Carlo calculations. Physica. 1969 May;42(3):388–397.
[32] Van Workum K, Yoshimoto K, de Pablo J, et al. Isothermal stress and elasticity tensors for ions and point dipoles using Ewald summations. Phys Rev E. 2005 Jun;71(6):061102-1–061102–6.
[33] Rowley LA, Nicholson D, Parsonage NG. Monte Carlo grand canonical ensemble calculation in a gas-liquid transition region for 12–6 Argon. J Comput Phys. 1975 Apr;17(4):401–414.
[34] Allen MP, Tildesley DJ. Computer simulation of liquids. New York (NY): Oxford University Press; 1989.
[35] Peterson OG, Batchelder DN, Simmons RO. Measurements of X-ray lattice constant, thermal expansivity, and isothermal compressibility of argon crystals. Phys. Rev. 1966 Oct;150(2):703–711.
[36] Barrett CS, Meyer L. X-ray diffraction study of solid argon. J Chem Phys. 1964;41(4):1078–1081.
[37] Ungerer P, Tavitian B, Boutin A. Applications of molecular simulation in the oil and gas industry: Monte Carlo Methods. Paris, France: Editions Technip; 2005.
[38] McDonald IR. NpT-ensemble Monte Carlo calculations for binary liquid mixtures. Mol Phys. 1972 Jan;23(1):41–58.
[39] Shinoda W, Shiga M, Mikami M. Rapid estimation of elastic constants by molecular dynamics simulation under constant stress. Phys Rev B. 2004 Apr;69(13):134103-1–134103-8.
[40] Van-Oanh N-T, Houriez C, Rousseau B. Viscosity of the 1-ethyl-3-methylimidazolium bis(trifluoromethylsulfonyl)imide ionic liquid from equilibrium and nonequilibrium molecular dynamics. Phys Chem Chem Phys. 2010;12(4):930–936.
[41] Kolb A, Dünweg B. Optimized constant pressure stochastic dynamics. J Chem Phys. 1999 Sep;111(10):4453–4459.
[42] Van Workum K, Gao G, Schall JD, et al. Expressions for the stress and elasticity tensors for angle-dependent potentials. J Chem Phys. 2006;125(14):144506-1–144506-10.
[43] Gusev AA, Zehnder MM, Suter UW. Fluctuation formula for elastic constants. Phys Rev B. 1996 Jul;54(1):1–4.
[44] Van Workum K, de Pablo JJ. Improved simulation method for the calculation of the elastic constants of crystalline and amorphous systems using strain fluctuations. Phys Rev E. 2003 Jan;67(1):011505-1–011505-5.
[45] Cowley ER. Some Monte Carlo calculations for the Lennard–Jones solid. Phys Rev B. 1983 Sep;28(6):3160–3163.
[46] Ray JR, Moody MC, Rahman A. Molecular dynamics calculation of elastic constants for a crystalline system in equilibrium. Phys Rev B. 1985 Jul;32(2):733–735.
[47] Ray JR, Moody MC, Rahman A. Calculation of elastic constants using isothermal molecular dynamics. Phys Rev B. 1986 Jan;33(2):895–899.
[48] Moeller HR, Squire CF. Ultrasonic velocities in solid argon. Phys Rev. 1966 Nov;151(2):689–693.
[49] Jones GO, Sparkes AR. Variation with temperature of the velocity of transverse elastic waves in solid argon. Philos Mag. 1964 Dec;10(108):1053–1057.
[50] Gsänger M, Egger H, Lüscher E. Determination of the elastic constants of argon. Phys Lett A. 1968 Oct;27(10):695–696.
[51] Keeler GJ, Batchelder DN. Measurement of the elastic constants of argon from 3 to 77 degrees K. J Phys C: Solid State Phys. 1970 Mar;3(3):510–522.
[52] Meixner H, Leiderer P, Lüscher E. Temperature dependence of the hypersonic velocity in a single crystal of argon. Phys Lett A. 1971 Oct;37(1):39–40.
[53] Hoover WG, Holt AC, Squire DR. Adiabatic elastic constants for argon. Theory and Monte Carlo calculations. Physica. 1969 Sep;44(3):437–443.
[54] Dobbs ER, Jones GO. Theory and properties of solid argon. Rep Prog Phys. 1957 Jan;20(1):516–564.
[55] Hill R. The elastic behaviour of a crystalline aggregate. Proc Phys Soc Sec A. 1952 May;65(5):349–354.
[56] Shirts MR. Simple quantitative tests to validate sampling from thermodynamic ensembles. J Chem Theory Comput. 2013 Feb;9(2):909–926.
[57] Rogge SMJ, Vanduyfhuys L, Ghysels A, et al. A comparison of barostats for the mechanical characterization of metal–organic frameworks. J Chem Theory Comput. 2015 Dec;11(12):5583–5597.
[58] Brookes CJ, Betteley IG, Loxston SM. Mathematics and statistics for students of chemistry, chemical engineering, chemical technology and allied subjects. Chichester (UK): Wiley; 1966.

Appendix 1. From Hooke to Voigt

The expression of the stress tensor element using implicit sum convention is:

$$\sigma_{\alpha\beta} = C_{\alpha\beta\mu\nu}\epsilon_{\mu\nu} \tag{A1}$$

where indices α, β, μ and ν are cartesian coordinates. Therefore, $\sigma_{\alpha\beta}$ is given by:

$$\begin{aligned}\sigma_{\alpha\beta} = {} & C_{\alpha\beta xx}\epsilon_{xx} + C_{\alpha\beta xy}\epsilon_{xy} + C_{\alpha\beta xz}\epsilon_{xz} \\ & + C_{\alpha\beta yx}\epsilon_{yx} + C_{\alpha\beta yy}\epsilon_{yy} + C_{\alpha\beta yz}\epsilon_{yz} \\ & + C_{\alpha\beta zx}\epsilon_{zx} + C_{\alpha\beta zy}\epsilon_{zy} + C_{\alpha\beta zz}\epsilon_{zz}\end{aligned} \tag{A2}$$

Using $\epsilon_{\mu\nu} = \epsilon_{\nu\mu}$ and $C_{\alpha\beta\mu\nu} = C_{\alpha\beta\nu\mu}$, we get:

$$\begin{aligned}\sigma_{\alpha\beta} = {} & C_{\alpha\beta xx}\epsilon_{xx} + 2C_{\alpha\beta xy}\epsilon_{xy} + 2C_{\alpha\beta xz}\epsilon_{xz} \\ & + C_{\alpha\beta yy}\epsilon_{yy} + 2C_{\alpha\beta yz}\epsilon_{yz} \\ & + C_{\alpha\beta zz}\epsilon_{zz}\end{aligned} \tag{A3}$$

If we introduce Voigt notation for $\sigma_{\alpha\beta}$, $\epsilon_{\alpha\beta}$ and $C_{\alpha\beta\mu\nu}$ elements where pairs of indices are replaced by simplets as $xx = 1$, $yy = 2$, $zz = 3$, $yz = 4$, $xz = 5$ and $xy = 6$, this expression can be conveniently put into a generalised Hooke's type expression (with $j = 1$–6)

$$\sigma_i = C_{ij}\epsilon_j \tag{A4}$$

if we write $\epsilon_6 = 2\epsilon_{xy}$, $\epsilon_5 = 2\epsilon_{xz}$ and $\epsilon_4 = 2\epsilon_{yz}$.

Appendix 2. Statistical errors

A.1. Explicit deformation computations

Each stiffness tensor element C_{ij} is computed from the slope of curves of σ_i vs. ϵ_j, assuming a simple linear regression. As usual, the slope s is computed as follows:

$$s = \frac{\sum_{a=1}^{n}\left(\sigma_{i,a} - \bar{\sigma}_i\right)\left(\epsilon_{j,a} - \bar{\epsilon}_j\right)}{\sum_{a=1}^{n}\left(\epsilon_{j,a} - \bar{\epsilon}_j\right)^2} = \frac{\mathrm{Cov}(\sigma_i, \epsilon_j)}{\mathrm{Var}(\epsilon_j)} \tag{A5}$$

where n is the number of data points.

The standard error of the regression slope s is expressed as follows:

$$\Delta_s = \frac{1}{\sqrt{n-2}}\left(\frac{\sum_{a=1}^{n}\sigma_{i,a}^2 - n\bar{\sigma}_i^2}{\sum_{a=1}^{n}\epsilon_{j,a}^2 - n\bar{\epsilon}_j^2} - s^2\right)^{1/2} \tag{A6}$$

The 95% confidence limits on the true value of s will be given using the Student's t distribution for the given number of degrees of freedom:

$$\mathrm{CL}_s = s \pm t_{(0.05,n-2)}\ \Delta_s \tag{A7}$$

Finally, the statistical error reported for C_{ij} computed using explicit strain is $\pm t_{(0.05,n-2)}\ \Delta_s$. This quantity should rather be called confidence interval, although the term statistical error is commonly used. More details can be found in [58].

A.2. Fluctuation in (NVT) or (NpT) simulations

For these simulations, we use the method of blocks [34]. The full set of data is divided into 10 equivalent sets, considered as statistically independent blocks. Average C_{ij} values are computed for each block and over the full set of data, and the standard error of the mean Δ_c is computed. Finally, the statistical error reported for C_{ij} computed from fluctuation methods is $\pm t_{(0.05,8)}\ \Delta_c$.